Integrated Strategy for Optimized Charging and Balancing of Lithium-ion Battery Packs

Galo D. Astudillo, Hamzeh Beiranvand, *Member, IEEE*, Federico Cecati, *Member, IEEE*, Christian Werlich, Andreas Würsig, Marco Liserre, *Fellow, IEEE*

***Abstract*—During fast charging of Lithium-Ion batteries (LIB), cell overheating and overvoltage increase safety risks and lead to faster battery deterioration. Moreover, in conventional Battery Management Systems (BMS), the cell balancing, charging strategy and thermal regulation are treated separately at the expense of faster cell deterioration. Hence, this paper proposes an optimized fast charging and balancing strategy with electro-thermal regulation of LIB packs. Thereby, the power dissipation constraints of the passive balancing are introduced in the proposed integrated optimal framework and cell balancing is achieved by bypassing the extra charging current. The electro-thermal model of the cells, along with a battery pack formed by a string of cells, is implemented. Extensive experiments are carried out to identify the coefficients for the Lithium-Ion cell model, i.e. Samsung-INR18650-20R, and the charging current trajectory as well as the balancing signals are generated with Model Predictive Control (MPC). The pack level simulations and experiments show that the proposed algorithm maintains the electro-thermal boundaries throughout the charging process, increasing the safe charge acceptance of the battery pack.**

***Index Terms*—Fast charging, battery pack, electro-thermal battery model, nonlinear Model Predictive Control.**

I. Introduction

THE Battery Management System (BMS) plays a critical role in Battery Energy Storage Systems (BESS) by providing cell monitoring, thermal management, cell balancing, charge control, battery safety and protection, state-of-health (SOH) and state-of-charge (SOC) estimation [1]. However, reports of explosions and fires on Electric Vehicles (EV) advocate for a better BMS design with improved battery state monitoring and regulation for extended lifetime [2]. This is particularly important for Lithium-Ion batteries (LIB), whose expansion has been hampered due to safety concerns, in which thermal runaway (TR) is the main factor [3]. On the application side on charging strategies, fast charging operates near the electro-thermal boundaries of LIB, making individual battery control a requirement. However, most evaluations of optimal charging strategies with electro-thermal boundaries in literature barely include more than one cell [4]–[6]. Yet, the single-cell optimal charging strategies do not include the discrepancies between cells caused by different aging and operating conditions, as well as manufacturing tolerances. Besides, the optimal current profile of a battery pack should incorporate the safe operation area (SOA) [7] and internal states of each cell.

Regarding to LIB charging, standard procedures such as constant-current (CC), constant-current constant-voltage (CCCV) or even multi-stage CCCV [8] are relatively simple to implement. In these methods, voltage/current limits can be ensured, but thermal regulation and balancing are assessed separately or not assessed at all. More complex and more effective charging strategies in closed-loop operation use the battery states as feedback and provide current, voltage, power, charge and thermal regulation [4], [9], [10]. To implement these strategies, modelling the battery dynamics and optimization algorithms are essential. Battery models could be classified into physical-based electrochemical models, electric equivalent circuit models and data-driven models [11]. Formulations based on equivalent circuit models (ECM) and lumped thermal models (LTM) combine low computational requirements, high accuracy, robustness and have also been widely evaluated in research. Once the model is selected, the charging profile should be optimized based on both the battery model and knowledge of the internal battery states.

With regards to the charging optimization algorithm, different approaches have been developed and are summarized by [4], [5]. In most methods, the optimal charging strategy is applied to a single cell, and very few exceptions consider a battery pack. Some of these exceptions include the works summarized on Table I. In particular, Pozzi et al. [14], [18] proposes the use of nonlinear Model Predictive Control (NMPC) to address aging, balancing and thermal regulation of the entire battery pack. This resulted in a faster charging time and safer thermal operation than the CCCV approach. However, either additional switches are required [14] or the discharge/dissipation constraints at a cell level are not considered [18]. Additional switches per cell increases the costs considerably, specially when the charging currents are relatively high, and the current dissipated by the shunt resistor is constrained by its power dissipation capabilities and the battery voltage. Moreover, an experimental evaluation of these MPC-based strategies is still pending and necessary due to the new challenges that simulations do not reveal.

The aforementioned limitations motivate the development and experimental evaluation of an integrated charging and balancing strategy that satisfies the thermal constraints at cell level. Consequently, we developed a NMPC-based formulation for an optimal charging of a battery pack with a string configuration without additional switches, considering the SOA, balancing, and energy dissipation limitations at a cell level. To achieve a faster charging time, the balancing is forced during the charging process, and the energy dissipated via the shunt resistor does not flow from the cell but from the charger. A simulation setup is developed based on 2 Ah Samsung INR18650-20R cylindrical cells. To evaluate the method, a cell model (ECM + ETM) is generated through extensive experimentation, and simulations compare the NMPC charg-

TABLE I
SUMMERY OF OPTIMAL CHARGING STRATEGIES FOR BATTERY PACKS

Authors	Battery Model	n Cells	Thermal Dynamics	Thermal Regulation	Evaluation	Est/Obs	Ageing	Control Time	Algorithm
Ouyang et al., 2018 [12]	ECM	3	no	no	Sim & Exp	no	no	L1=600s, L2=60s, VTs=0.5s	2-L Opt
Ouyang et al., 2020 [13]	ECM	10	no	no	Sim & Exp	yes, LO	no	L1=300s, L2=1s	2-L Opt
Pozzi et al., 2020 [14]	ELM	6	yes	**yes**	Sim	yes, EKF	yes	10s	NMPC
Ouyang et al., 2022 [15]	ECM	4	no	no	Sim & Exp	no	no	600s	2-L Opt
Chen et al., 2022 [16]	ECM	4	no	no	Sim & Exp	no	no	1s	QP
Yan et al., 2024 [17]	ECM	4	no	no	Sim & Exp	no	no	1s	DRL

ing strategy and the standard CCCV with passive balacing (CCCV+PB) in a battery pack. Moreover, a 4-cell battery pack is built and tested in the laboratory to corroborate the results in hardware by integrating the NMPC strategy and Unscented Kalman Filter-based (UKF) battery states estimation. The proposed charging strategy includes power dissipation constraints, electro-thermal regulation, fast-charging, charge balance and the corresponding evaluation in hardware and simulation.

The main contributions of this paper are the following:

- Development of an efficient charging approach for the battery pack that ensures electro-thermal regulation at the individual cell level, while also addressing current limitations and considering parameter variations between different cells.
- Simultaneous cell charge balancing and fast charging.
- Ready-to-implement charging strategy that could be applied to existent BESS to balance the charge and control the core temperature of the cells.
- Evaluation of the optimal charging strategy through simulation and in an experimental setup considering the integration of the NMPC and the battery states estimator.

Consequently, this research contributes in the development of more reliable and more efficient BMS for EV and BESS applications.

II. ELECTRO-THERMAL MODEL OF BATTERY STRING

A. Battery Model

The simplified model of the cell using an equivalent electric circuit is presented in Fig 2 (a). The battery polarization voltage is modeled with 1-RC circuit (R_p, C_p) and the battery internal resistance (R_o). The open-circuit voltage (OCV) is represented with a variable voltage source (v_{ocv}), and the SOC (χ) is retrieved via Coulomb counting, i.e.:

$$\dot{v_c} = -\frac{v_c}{R_p C_p} + \frac{i}{C_p} \tag{1}$$

$$\dot{\chi} = \frac{\eta i}{C_{bat}} \tag{2}$$

$$v = iR_o + v_c + v_{ocv} \tag{3}$$

The battery parameters are temperature dependent and/or SOC dependent. The dependencies of the parameters are mostly represented by polynomial functions, assuming a thermal decoupling during the parametrization:

$$v_{ocv}(\chi, T) = \sum_{l=0}^{8} a_l \chi^l (b_0 + b_1 T + b_2 T^2) \tag{4}$$

$$R_o(\chi, T) = \sum_{l=0}^{1} c_l \chi^l (d_0 + d_1 T + d_2 T^2) \tag{5}$$

$$R_p(T) = e_0 + e_1 T + e_2 T^2 \tag{6}$$

$$C_p(T) = f_0 + f_1 T + f_2 T^2 \tag{7}$$

$$C_{bat}(T) = g_0 + g_1 T \tag{8}$$

The thermal model for a cylindrical cell is shown in Fig. 2 (b). The core temperature, surface temperature and coolant/ambient temperature are T_c, T_s and T_f, respectively. The thermal resistance and heat capacity are R_c and C_c between the core and the surface, and R_u and C_s between the surface and the coolant/exterior.

$$C_c \frac{dT_c}{dt} = Q + \frac{T_s - T_c}{R_c} \tag{9}$$

$$C_s \frac{dT_s}{dt} = \frac{T_f - T_s}{R_u} - \frac{T_s - T_c}{R_c} \tag{10}$$

The heat generation in the battery can be decomposed in two parts: reversible (Q_{rrev}) and irreversible (Q_{irrev}) heat. When the charging current is high, the reversible heat could be neglected [5], and the total heat is:

$$Q \sim Q_{irrev} \sim i(v - v_{ocv}) \sim i^2 R_o + i v_c \tag{11}$$

B. Battery String Model

The battery pack has a string configuration with a single driving current i_{opt} and a shunt resistor (R_d) attached to each cell (see Fig. 1). In this scenario, the total string voltage is given by the summation of the individual cell voltages (v_j):

$$v_{string} = \sum_{j=1}^{n} v_j \tag{12}$$

To counteract the cell discrepancies, a passive balancing circuit is implemented. There are mainly two balancing approaches: active and passive [20]. Passive balancing (PB) uses a resistor to dissipate the battery unbalance energy at the expense of heat and safety issues [21]. Conventionally, a simple current bypass approach could also be implemented via a shunt resistor/transistor attached to the cell(s). On the other hand, active balancing (AB) strategies use power electronics to transfer energy between cells achieving higher efficiency

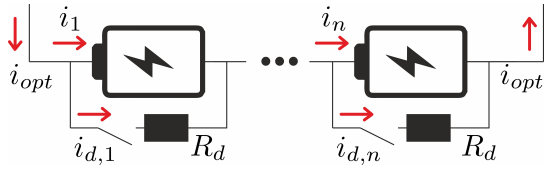

Fig. 1. Battery pack with cells in series and single driving current i_{opt}.

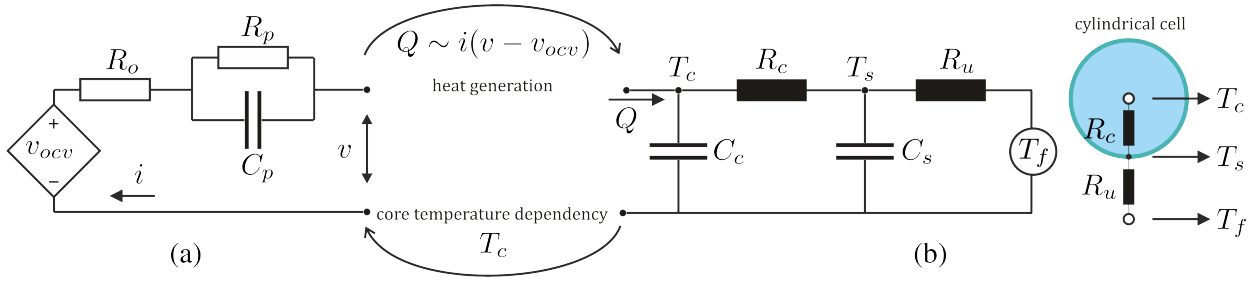

Fig. 2. Battery Model: (a) Equivalent circuit model (ECM) and (b) Lumped thermal model (LTM). The power losses, Q, generated in ECM is fed into LTM and the calculated core temperature (top-view of cylindrical cell), T_c is the feedback to change the temperature-dependant parameters. Thereby, a complete electro-thermal model for the cell is achieved.

than PB at the expense of more components, higher costs, and complexity [21]. The superior efficiency of AB is more prominent in presence of different cell aging, yet it is relatively low on new cells [22]. If homogeneous ageing is achieved, the advantages of AB over PB are reduced. Therefore, it can be beneficial to counteract the effects of heterogeneous aging on battery packs with PB. To accomplish this, the core temperature of the cells need to be regulated, since unregulated temperature increase impacts negatively the SOH during cycle aging [23]. Hence, PB with homogeneous cell ageing could reduce implementation costs without compromising efficiency.

On the other hand, the thermal model is based on [24] (see Fig. 3). Note that the ECM of each cell does not change; however, the thermal coupling ($Q_{cc,j}$) is now introduced on the thermal model. The coldest cell is the first cell on the coolant path and also the first cell of the string, while the last one is the warmest one. The thermal model of each cell j of the string is given below:

$$C_{c,j}\frac{dT_{c,j}}{dt} = Q_j + \frac{1}{R_{c,j}}(T_{s,j} - T_{c,j}) \tag{13}$$

$$C_s\frac{dT_{s,j}}{dt} = \frac{1}{R_{u,j}}(T_{f,j} - T_{s,j}) - \frac{1}{R_{c,j}}(T_{s,j} - T_{c,j}) + Q_{cc,j} \tag{14}$$

$$Q_{cc,j} = \begin{cases} \frac{1}{R_{cc}}(T_{s,2} - T_{s,1}) & \text{if } j = 1 \\ \frac{1}{R_{cc}}(T_{s,j-1} - T_{s,j+1} - 2T_{s,j}) & \text{if } j = 2, ..., n-1 \\ \frac{1}{R_{cc}}(T_{s,n-1} - T_{s,n}) & \text{if } j = n \end{cases} \tag{15}$$

Moreover, the coolant temperature on each cell is given by:

$$T_{f,j} = \begin{cases} T_{f,in} & \text{if } j = 1 \\ T_{f,j-1} + \frac{1}{R_{u,j}C_f}(T_{s,j-1} - T_{f,j-1}) & \text{if } j = 2, ..., n \end{cases} \tag{16}$$

Two coefficients are introduced: the conduction resistance between cells R_{cc} and the coolant flow capacity C_f. In addition, it is assumed that all the cells have the same thermal parameters. The thermal model of the string is presented in Fig. 3.

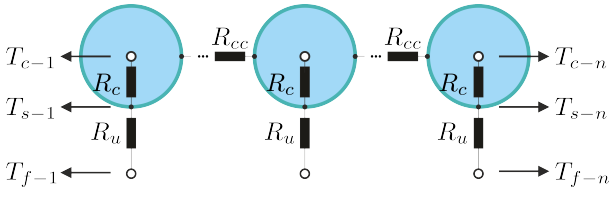

Fig. 3. Thermal model of the battery pack (top-view of cylindrical cells) [19].

III. Optimal Problem Formulation

The voltage, current, temperature and power dissipation limits of each cell and shunt resistor (R_d) should be maintained at all times. This poses a challenge in the generation of the optimal charging current due to the heterogeneous states of the cells. In addition, careful consideration should be given to R_d before bypassing a portion of the string current while charging. The requirements for the charging current and bypassing current are threefold:

1) The shunt resistor and switching device have limited power capabilities, and are dimensioned below the charge acceptance of the battery. Therefore, the discharging current should comply with the dissipation power limits.
2) The current through R_d depends on the battery terminal voltage. Therefore, a dynamic current assignation to each cell is limited by the string current and the maximum current that can be dissipated by the resistor given the terminal voltage during charging mode.
3) To reduce the balancing and charging time, the cells should not be discharged. Consequently, the string current should have a lower limit so that the cells are always charging even when the bypass resistor is activated.

The three aforementioned requirements can be fulfilled by means of the following procedure, starting by determining the minimum charging current. By using Kirchhoff's law for cell j, we have:

$$i_{opt} = i_j + i_{d,j} = i_j + \frac{v_j}{R_d} \quad for\, j = 1, ..., n \tag{17}$$

If the string current is smaller than the current through R_d, then the cell will discharge. Hence, the value of the minimum charging current should be defined, so that the cell remains in charging mode/positive polarization (i.e. $i_j \geq 0$). From Eq. (17) and (3) we have:

$$i_{opt} = i_j + \frac{1}{R_d}(i_j R_o + v_{c,j} + v_{ocv}) \tag{18}$$

$$\frac{1}{(R_d + R_o)}(i_{opt} R_d - (v_{c,j} + v_{ocv})) = i_j \geq 0$$

$$i_{opt}R_d - (v_{c,j} + v_{ocv}) \geq 0$$
$$i_{opt}R_d \geq v_{max} \geq v_{c,j} - v_{ocv}$$
$$i_{opt} \geq \frac{v_{max}}{R_d} = i_{min} \tag{19}$$

Here, Eq. (19) establishes a lower boundary for the minimum string current. Now, we are looking for the minimum current that will pass through the cell j when the shunt resistor is activated:

$$i_{jmin} = i_{opt} - \frac{1}{(R_d)}(i_{jmin}R_o + v_{c,j} + v_{ocv}) \tag{20}$$

solving for i_{jmin} leads to:

$$i_{jmin} = \frac{1}{(R_d + R_o)}(i_{opt}R_d - (v_{c,j} + v_{ocv})) \tag{21}$$

With Eq. (21) and i_{opt}, the current range for i_j is:

$$\frac{1}{(R_d + R_o)}(i_{opt}R_d - (v_{c,j} + v_{ocv})) \leq i_j \leq i_{opt} \tag{22}$$

There is, however, one more boundary for the shunt resistor, which is given by the maximum dissipation power P_d:

$$(i_{opt} - i_j)(v_{c,j} + v_{ocv} + i_j R_o) \leq P_d \tag{23}$$

In essence, Eq. (19), (22), and (23) gather the conditions to use the shunt resistor to bypass the current during charging and satisfy the requirements 1) to 3). If the resistor is dimensioned to dissipate more power than the power generated at the maximum battery voltage (i.e. $R_d P_d > v_{max}^2$), then Eq. (23) can be omitted. In practice, the desired current i_j is realized by pulse width modulation (PWM), with the duty cycle (D) as the ratio of the desired current and the maximum current that should be drained by the shunt resistor. This is determined as follows:

$$D = \frac{i_{d,j}}{i_{opt} - i_{jmin}} = \frac{i_{opt} - i_j}{i_{opt} - i_{jmin}} \tag{24}$$

Here, $i_j \leq i_{opt}$ are both generated by the control law, while i_{jmin} is given by Eq. (21).

The charging current for the string and each cell of the battery pack is retrieved iteratively by the solving a finite-horizon optimization problem. The cost function on the NMPC framework with an horizon H is presented below:

$$J_H = m(\boldsymbol{x}[H]) + \sum_{k=0}^{H-1} l(\boldsymbol{x}[k], \boldsymbol{i}[k]) + r(\boldsymbol{i}[k]) \tag{25}$$

The states vector at the time step k is the following:

$$\begin{aligned}\boldsymbol{x}[k] = (&\chi_1[k], v_{c,1}[k], T_{c,1}[k], T_{s,1}[k], \ldots, \\ &\chi_j[k], v_{c,j}[k], T_{c,j}[k], T_{s,j}[k], \ldots, \\ &\chi_n[k], v_{c,n}[k], T_{c,n}[k], T_{s,n}[k])^T\end{aligned} \tag{26}$$

Here, n is the total number of cells. The input vector $\boldsymbol{i}$ at the time step k has $n+1$ elements, including i_{opt}:

$$\boldsymbol{i}[k] = \left(i_1[k] \ldots i_j[k] \ldots i_n[k], i_{opt}[k]\right)^T \tag{27}$$

The aim is to minimize J_H satisfying the system dynamics and electro-thermal constraints for each time step k and each cell j:

$$\min_{\boldsymbol{i}} J_H \tag{28a}$$
$$s.t.: \ \forall\, k \in \{0, ..., H-1\}$$
$$\boldsymbol{x}_{k+1} = f(\boldsymbol{x}[k], \boldsymbol{i}[k]) \tag{28b}$$
$$i_{min} \leq i_{opt}[k] \leq i_{max} \tag{28c}$$
$$v_{min} \leq v_j[k] \leq v_{max} \tag{28d}$$
$$\chi_{min} \leq \chi_j[k] \leq \chi_e \tag{28e}$$
$$(i_{opt}[k] - i_j[k])(v_{c,j}[k] + v_{ocv} + i_j[k]R_o) \leq P_d \tag{28f}$$
$$max(0, i_{jmin}[k]) \leq i_j[k] \leq i_{opt}[k] \tag{28g}$$
$$for\ j = 1, ..., n$$

It is important to mention that the boundaries of the inequality constraints (28f) and (28g) are dynamic (the other inequalities have fixed boundaries given by the manufacturer). This is due the increase in a degree of freedom resulting from $i_{opt}[k]$. Moreover, the model parameters and their dependencies on the core temperature and/or SOC should also be included.
On the other hand, the terminal cost $m(\boldsymbol{x}[H])$, the running cost $l(\boldsymbol{x}[k], \boldsymbol{i}[k])$, and the penalty $r(\boldsymbol{i}[k])$ for the control input change are detailed below:

$$l(\boldsymbol{x}[k], \boldsymbol{i}[k]) = \alpha\sigma_l(\boldsymbol{x}[k]) \tag{29}$$

$$m(\boldsymbol{x}[H]) = \beta\sigma_m(\boldsymbol{x}[H]]) \tag{30}$$

$$r(\boldsymbol{i}[k]) = (\boldsymbol{i}[k] - \boldsymbol{i}[k-1])^T R(\boldsymbol{i}[k] - \boldsymbol{i}[k-1]) \tag{31}$$

There are two functions (σ_l, σ_m), and each one of them has a fixed weight (α, β), respectively. In addition, there is a penalty (R) to prevent an abrupt change in the input current.

The function σ_l penalizes the SOC unbalances between cells:

$$\sigma_l(\boldsymbol{x}[k]) = \frac{1}{n}(|\chi_1[k] - \chi_n[k]|^2 + \sum_{j=1}^{n-1} |\chi_j[k] - \chi_{j+1}[k]|^2) \tag{32}$$

The function σ_m penalizes the difference between the estimated core temperature and the target core temperature:

$$\sigma_m(\boldsymbol{x}[k]) = \frac{1}{n}\sum_{j=1}^{n}(T_{c,j}[k] - T_{c-max})^2 \tag{33}$$

This simple formulation facilitates the generation of a fast charging current that is bounded by desired maximum core temperature T_{c-max}. For this, the ambient temperature should always be kept below the desired T_{c-max}, which is true for most applications. As a result, the current is regulated and the SOC of the cells are homogenized simultaneously.

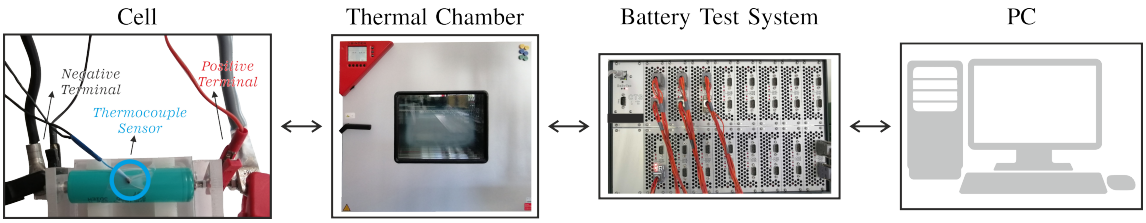

Fig. 4. Testbench for battery parametrization.

IV. Experimental Setup and Model Parametrization

The test cell is the Samsung INR18650-20R. The details of the cell are shown on Table II. The model presented here is not unique, and can be adjusted for different battery chemistries. The general procedure to obtain the coefficients of different ECM is similar between different models [25]. This paper uses a procedure akin to [26], and includes the temperature dependencies as in [27], assuming only 1-RC branch and no parameter variation between charging/discharging.

TABLE II
Parameters of the cell: Samsung INR18650-20R

Chemistry	C_{bat}	v_{min}	v_{max}	$i_{max} \uparrow$	$i_{max} \downarrow$	T_{rec}
NCA	2Ah	2.5V	4.2V	4A	22A	45^{o}C

Two new cells (A and B) were used for the model parametrization. Cell A was used to obtain the coefficients of the ECM at different temperatures: 5 ^{o}C, 25 ^{o}C and 45 ^{o}C, respectively. Cell B was used to obtain the coefficients of the thermal model. The test bench is shown in Fig 4. The battery cycler is a BaSyTec CTS 32 Standard and the model of the thermal chamber is Binder MK-240. The pulse test at different SOC (χ) was used for obtaining the battery internal resistance (R_o), open-circuit voltage (v_{ocv}) and the RC coefficients during the transient response. The following procedure is repeated on cell A at the aforementioned temperatures, considering that the cell is initially fully charged:

1) CC discharge at 1C until $v \leq v_{min}$.
2) CCCV charge at 1C until $i_{charging}$ ≤0.02C.
3) 2:00h pause.
4) Discharging pulse test with 1C for 6min + 2:00h pause.
5) Charging pulse test with 1C for 6min + 2:00h pause.

An example of this procedure at 5^{o}C is shown in Fig. 5. The experiment on cell D was performed at 20^{o}C inside the climate chamber. The current, voltage and surface temperature are shown in Fig. 6, and the procedure is presented below:

1) CCCV charge at 1C until $i_{charging}$ ≤0.02C.
2) 2:00h pause.
3) CC discharge at 2C until $v \leq v_{min}$.
4) 3:30h pause.
5) CCCV charge at 2C until $i_{charging}$ ≤0.02C.
6) 3:30h pause.

The electro-thermal model for this battery is the same for both the simulation and the NMPC formulation, except for one parameter: v_{ocv}. Given that the cells will operate with $\chi \geq 0.1$, and that there are no significant differences on the

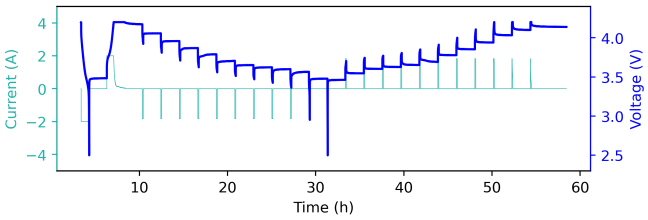

Fig. 5. Sample of pulse test at 5 ^{o}C and different SOC.

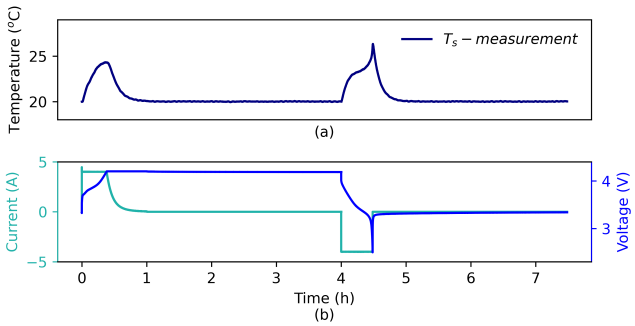

Fig. 6. (a) Measured surface temperature (T_s) and (b) the charging and discharging pulses with 2C-rate.

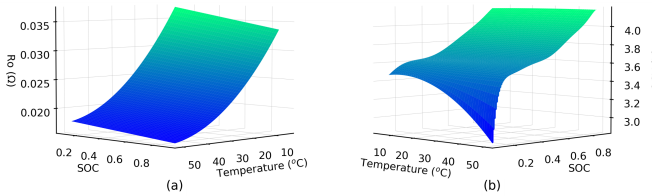

Fig. 7. Model parameters: (a) Internal battery resistance (R_o) and (b) open-circuit voltage (v_{ocv}) as a function of the state of charge and temperature.

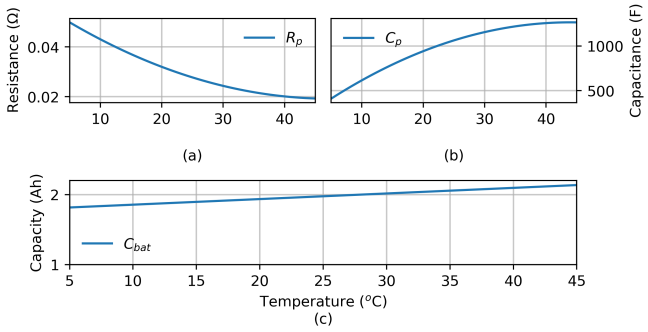

Fig. 8. RC parameters and battery capacity as a function of the state of temperature.

v_{ocv} above the aforementioned SOC at different temperatures, the thermal influence over v_{ocv} is neglected only on the NMPC formulation. The resulting R_o and v_{ocv} are shown in Fig. 7 (a) and (b), respectively; while the temperature dependency of

TABLE III
COEFFICIENTS FOR THE ECM AND LTM

Coef	Value	Coef	Value	Coef	Value	Coef	Value	Coef	Value	Coef	Value
a_0	3.390789	a_5	-296.6923	c_1	-0.002149	e_1	-1.62E-3	g_0	1.77666	C_s	44
a_1	0.437158	a_6	190.4799	d_0	2.240193	e_2	1.709E-5	g_1	0.008	R_{cc}	0.2
a_2	12.39648	a_7	-45.21235	d_1	-0.046317	f_0	176.5399	R_c	6.5	C_f	2.6
a_3	-83.03621	a_8	-1.925143	d_2	4.1684E-4	f_1	49.55106	C_c	25		
a_4	224.3434	c_0	0.018601	e_0	0.0575671	f_2	-0.563887	R_u	4.5		

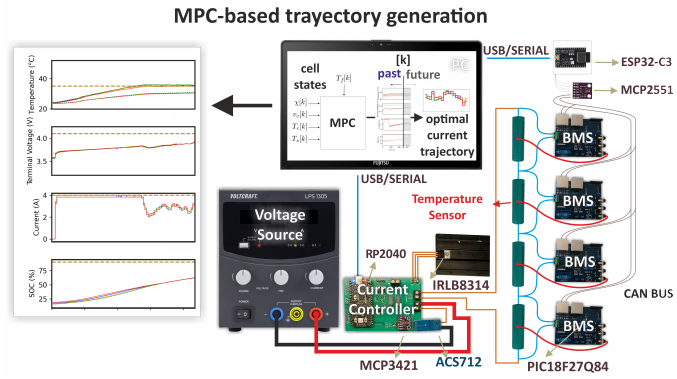

Fig. 9. Schematic of the prototype for evaluation of the charging strategy in hardware.

R_p, C_p and C_{bat} is shown in Fig. 8.

Moreover, the thermal coefficients are adjusted so that the difference between the measured surface temperature (T_S^*) and the model-given surface temperature (T_s) is minimal, following a similar procedure presented in [24], and using $i(v - v_{ocv})$ instead of i^2R_o. During this experiment, the ambient temperature T_f is kept constant inside the climate chamber.

The coefficients for both the ECM and LTM are presented in Table III. Note that C_f and R_{cc} dependent on the battery pack configuration and geometry. However, for simulation purposes, these two values were taken from [19].

A. Battery Management System (BMS)

A BMS has been built to validate the simulation results in hardware. For this task, the microntroller ($PIC18F27Q84$ from Microchip Technology) is programmed to consume low energy and provide the required peripherals such as the CAN bus interface, 12-bit ADC channels, and stand alone PWM. A setup containing four cells and a BMS for each cell was developed. The schematic of the setup is presented in Fig. 9. The BMS provides information about the internal battery states, namely the state of charge (χ), the polarization voltage (v_c), the increase in the battery resistance (δR), the battery core temperature (T_c) and surface temperature (T_s). Moreover, the terminal voltage and surface temperature of each cell are measured by each BMS. The estimation algorithm used hereof is the Unscented Kalman Filter (UKF), and it requires two additional inputs, namely the ambient/coolant temperature (T_f) and the cell current. These two inputs are measured separately, and transmitted via the CAN bus. Moreover, a bypass circuit (resistor + switch) in each BMS regulates the average bypass current via a PWM signal. Hence, the input current of each cell is equal to difference between the branch current and the bypass average current. As shown in Fig. 9, the control signal that sets the reference in the current source comes from the control algorithm. Similarly, the PWM control signal for each BMS is also commanded by the control algorithm. Once the internal battery states are computed, the data is transmitted via the CAN bus to the control algorithm. As a result, the close-loop operation of the control strategy and estimation is achieved. Aditionaly, it is worth mentioning that even though we use one BMS per cell, a bigger BMS could have been built to connect and balance many cells simultaneously. Therefore, the proposed approach can be applied to already operational BEES with PB and a string configuration.

V. RESULTS

The charging strategy is evaluated on simulation and on a real setup. The closed-loop control was implemented in Python 3.10 using a Model Predictive Control Toolbox (do-mpc, [28]), as well a symbolic framework for nonlinear optimization and algorithmic differentiation (CasADi, [29]) and an optimization package for large scale nonlinear continuous systems (IPOPT, [30]). As previously mentioned, the real setup uses the Unscented Kalman Filter for estimating the internal states of the cells.

A. Simulation results

A 10-cell battery pack is used for the simulation. Two scenarios are considered: (a) standard CCCV+PB balancing and (b) NMPC with bypass resistors. In both scenarios, the same initial conditions and boundaries were assumed and are summarized on Table IV. Note that the initial state-of-charge (χ_o) is randomly generated between 18% and 22%, and a random bias has also been added to the battery capacity to simulate a non-homogeneous capacity-defined SOH ($C_{bat}\pm$ 0.05Ah). The charging stops when the target χ_e is reached. Here, T_{ctr} is the controller time. The NMPC uses an horizon of $H = 3$, and the values of the weights are: $\alpha = 10^6$, $\beta = 10^2$, $R = 2$. The solver implements hard constraints and the second order collocation method.

In the first scenario with CCCV+PB balancing (see Fig. 10), the current is fixed during the CC region, and it starts to decrease during the CV region. Here, no thermal regulation occurs. Note that we have balanced the SOC instead of the terminal voltages because of its higher accuracy to provide a better comparison. Balancing while charging with standard

TABLE IV
SIMULATION PARAMETERS

Parameter	Value	Parameter	Value	Parameter	Value
i_{min}	0.158A	H	3	T_{c-max}	40°C
v_{max}	4.10V	χ_o	20±2%	R_d	10Ω
T_{ctr}	10s	χ_e	90%	P_d	0.65W
T_{tot}	3500s	C_{bat}	2.0±0.05Ah	n	10

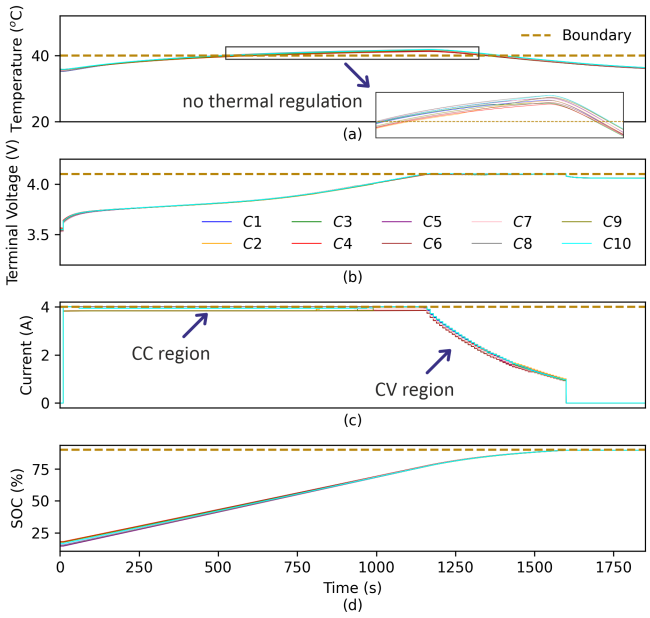

Fig. 10. Charging from 18%-22% to 90% with CCCV+PB. The (a) core temperature, (b) terminal voltage, (c) current, and (d) SOC of each cell.

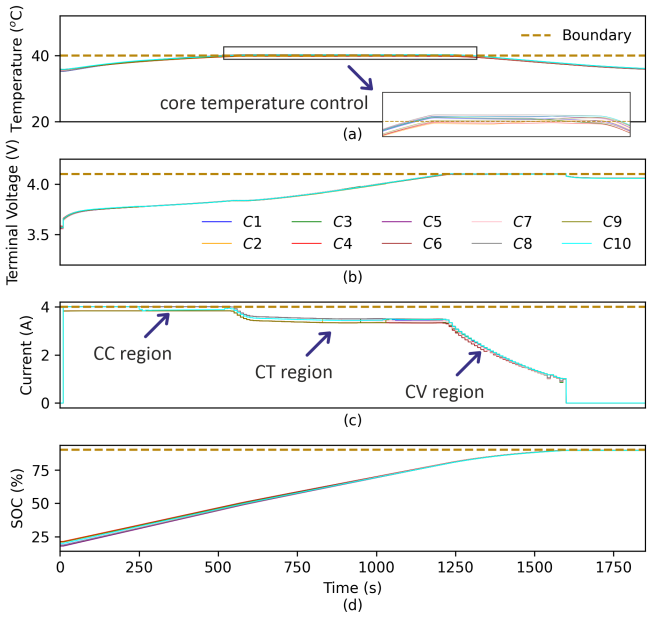

Fig. 11. Charging from 18%-22% to 90% with NMPC. The (a) core temperature, (b) terminal voltage, (c) current, and (d) SOC of each cell.

circuits (e.g. voltage balancing) requires careful consideration, specially when the variability of the internal resistance leads to greater voltage differences between the cells. Hence, voltage balancing usually occurs when low C-rates are applied, or when the terminal voltage reaches certain upper threshold. In contrast, SOC balancing requires an estimator.

On the other hand, the proposed strategy (see Fig. 11) protects the cells from overheating, reducing its impact on capacity loss (and therefore accelerated ageing) due to unregulated temperature [23]. This occurs due to the current

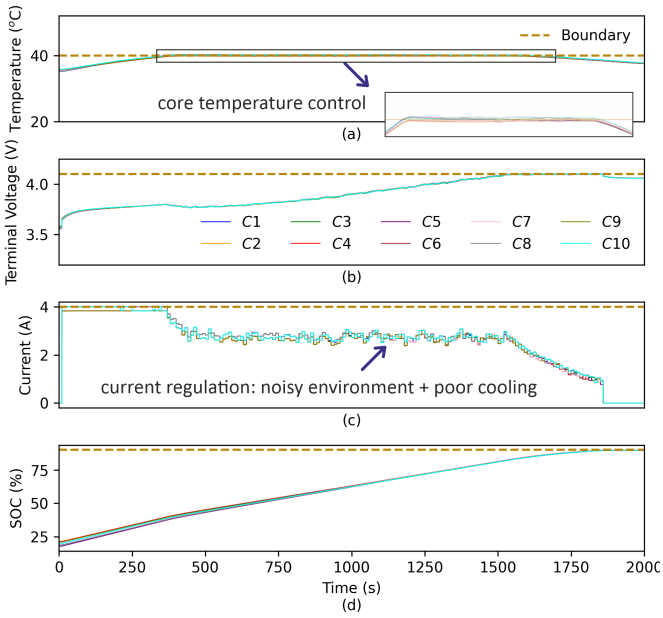

Fig. 12. Charging from 18%-22% to 90% with NMPC (noisy environment & poor cooling). The (a) core temperature, (b) terminal voltage, (c) current, and (d) SOC of each cell.

regulation provided by the NMPC and the constant temperature (CT) region. Note that it decides what switches to turn on/off to satisfy the charging and balancing goals, as well as the thermal constraints. Moreover, the desired maximum core temperature is now a design parameter, providing a framework for extending battery life time and efficiency when operating at the temperature at which the internal resistance is minimal.

The charge balancing is observed during the entire charging procedure, where the SOC is being homogenized in all the cells without stopping the current flow from the charger. In addition, the source of the power dissipation is not the cell but the charger, reducing the stress on the cells. This is accomplished by maintaining the string current above the minimum charging current to avoid negative battery polarization. However, it is also necessary to evaluate the controller in a noisy environment and including poor cooling conditions (greater thermal resistance and smaller thermal capacitance). Hence, random noise is added to the internal battery states. The additive noise is randomly generated within ± 0.001, ± 0.001V, $\pm 0.3^o$C, and $\pm 0.2^o$C for χ, v_c, T_c, and T_s, respectively.

Thus, the simulation results are shown in Fig. 12. The duty cycle of the bypass resistors of the latter experiment are presented in Fig. 13. Note that the duty cycle does not exceed 0.55. This is the result of constraining the maximum power dissipation capability of each cell. The core temperature slightly exceeded the 40 ^{o}C by a maximum of 0.30 ^{o}C. This is expected due to the aforementioned mismatch between the thermal coefficients between the model and the environment with poor cooling.

To achieve reduced balancing times, more power (higher value of P_d) should be allowed to be dissipated by the bypass resistor R_d, but the Joule effect in the resistor may require additional dissipation, such as active cooling. Hence, sizing the resistor is always a trade-off between balancing speed

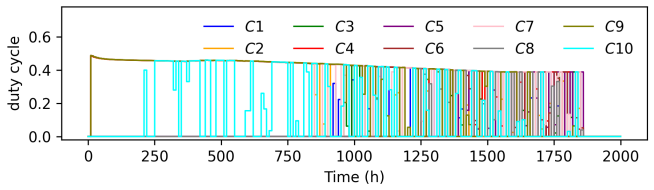

Fig. 13. Bypass current to duty cycle (D) mapping for each bypass resistor R_d (noisy environment & poor cooling).

and dissipation capabilities. By bypassing the charging current via R_d, the cells do not dissipate energy, and the overall energy needed to achieve the target SOC is also minimized. This occurs because the NMPC does not require to discharge the cell with the highest SOC down to the level of the cell with the lowest SOC. On the contrary, during charging, the cells with the lowest SOC receive more current than the cells with highest SOC, since the latter bypass part of the current, avoiding the need to discharge and recharge.

B. Hardware test results

The evaluation of the charging strategy on hardware is two-fold, considering the same charging goals presented in the previous section on Table IV, with the exception of the maximum allowed core temperature (T_{c-max}) and the number of cells ($N = 4$). The surface and core temperature, as well as the initial SOC are different on each case. For a more realistic validation, the battery model embedded in the BMS does not contain a priori information about the battery capacity and previous battery use, and no fine-tuning was used to match the battery model coefficients to each cell. The maximum core temperature was set to 40^oC and 35^oC in the first and second test, respectively. The second test has been done to demonstrate the controller action in a demanding scenario in which the charging process starts almost right after a discharge occurred and a lower core temperature is desired. In this test, 35^oC is close the temperature at which the internal resistance is minimal. The ambient temperature was kept at 22^oC throughout the experiments.

The initial states for each scenario are presented below:

- Experiment A: $T_s \sim (28.0^oC - 28.7^oC)$, $T_c \sim (31.3^oC - 32.5^oC)$, $\chi \sim (16.1\% - 19.4\%)$
- Experiment B: $T_s \sim (25.9^oC - 26.4^oC)$, $T_c \sim (28.6^oC - 29.2^oC)$, $\chi \sim (15.5\% - 18.0\%)$

The experiments are shown in Fig. 14 (Test A) and Fig. 15 (Test B), respectively. Note that in real-life applications the battery pack is usually charged soon after a previous use (e.g. the discharge of the BEES or EV), resulting in higher initial battery temperatures. Hence, the authors consider important to show these two cases for validation purposes. The algorithm stops when the $\chi > 0.90$ has been reached by all the cells. The electro-thermal regulation and charge balancing is present in both scenarios.

C. Algorithm Tuning Considerations

The tuning of the coefficients for solving the optimization problem (i.e. Eq. (25)) was achieved through manual search,

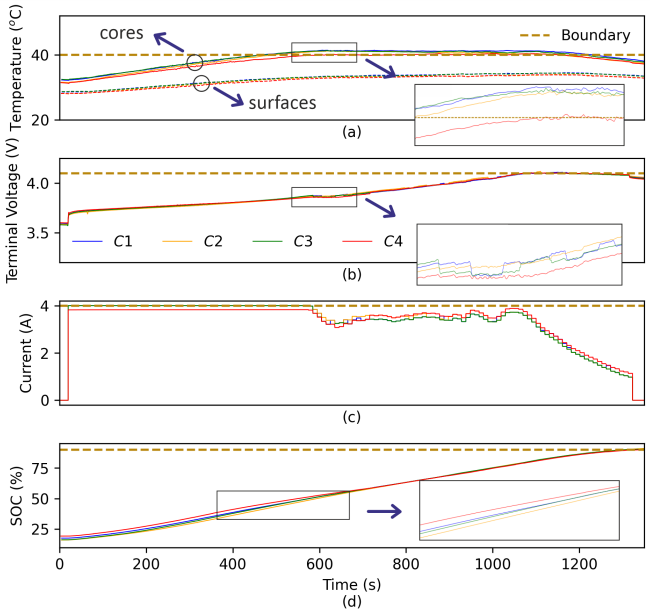

Fig. 14. Experiment A: charging with NMPC with $T_{c-max} = 40^oC$. The (a) temperature, (b) terminal voltage, (c) current, and (d) SOC of each cell.

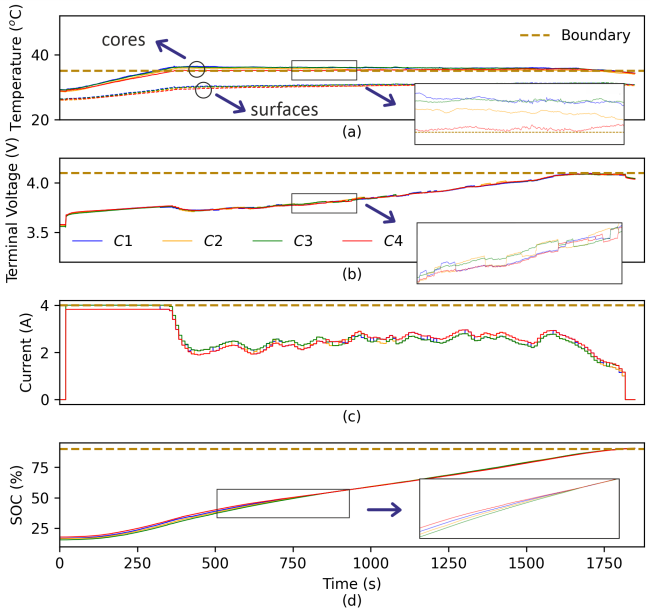

Fig. 15. Experiment B: Charging with NMPC with $T_{c-max} = 35^oC$. The (a) temperature, (b) terminal voltage, (c) current, and (d) SOC of each cell.

however other hyper-parameter tuning strategies such as genetic algorithms could be used instead. In this context, high values were employed as they led to a quicker convergence time of the solver. To analyze the scalability of the charging strategy, additional simulation tests were carried out considering 100 cells and the same aforementioned initial conditions and charging goals. The software was executed on a laptop with a Core i5-1135G7 2.40GHz processor, 16 GB of RAM and Windows 11. In the worst case, the solver found a charging strategy in less than 2s. The mean solver time was 1.07 s. These values are conservative and have been repeatedly found throughout most simulations. Since the control time was 10 s, this approach is suitable for larger battery systems.

VI. Conclusions

This paper presented an integrated charging and balancing strategy for LIBS packs with a string configuration. This framework considered the charging, balancing, and the system limitations in the generation of an optimal current profile for each cell and the battery pack employing NMPC. In the standard CCCV approach overheating may occur, accelerating the cell aging and increasing safety risks. Moreover, due to cell discrepancy, a balancing strategy is required and this increases the charging time when it is not considered during charging. In contrast, the proposed approach generates a charging and balancing current simultaneously and provides thermal regulation, maintaining the battery in the safe operational area. In addition, the inclusion of the desired core temperature during charging enhances safety, extends battery life time, and can increase efficiency by operating at the temperature with lowest internal resistance. The methodology was evaluated on a 10-cell battery pack in simulation and on a 4-cell battery pack in a real setup. For this, a coupled electro-thermal model of a commercial 2Ah battery was developed and tested. The study case shows the successful SOC homogenization and the desired core temperature tracking on all cells. Further works may consider thermal-gradient reduction as part of the optimization function, and re-configurable cells for faster balancing time.

References

[1] H. Rahimi-Eichi, U. Ojha, F. Baronti, and M.-Y. Chow, "Battery Management System: An Overview of Its Application in the Smart Grid and Electric Vehicles," *IEEE Industrial Electronics Magazine*, vol. 7, no. 2, pp. 4–16, Jun. 2013.

[2] P. Sun, R. Bisschop, H. Niu, and X. Huang, "A Review of Battery Fires in Electric Vehicles," *Fire Technology*, vol. 56, no. 4, pp. 1361–1410, Jul. 2020.

[3] X. Feng, D. Ren, X. He, and M. Ouyang, "Mitigating Thermal Runaway of Lithium-Ion Batteries," *Joule*, vol. 4, no. 4, pp. 743–770, Apr. 2020.

[4] C. Chen, Z. Wei, and A. C. Knoll, "Charging Optimization for Li-Ion Battery in Electric Vehicles: A Review," *IEEE Transactions on Transportation Electrification*, vol. 8, no. 3, pp. 3068–3089, Sep. 2022.

[5] N. Wassiliadis, J. Schneider, A. Frank, L. Wildfeuer, X. Lin, A. Jossen, and M. Lienkamp, "Review of fast charging strategies for lithium-ion battery systems and their applicability for battery electric vehicles," *Journal of Energy Storage*, vol. 44, p. 103306, Dec. 2021.

[6] P. Makeen, H. A. Ghali, and S. Memon, "A Review of Various Fast Charging Power and Thermal Protocols for Electric Vehicles Represented by Lithium-Ion Battery Systems," *Future Transportation*, vol. 2, no. 1, pp. 281–299, Mar. 2022.

[7] W. Waag, C. Fleischer, and D. U. Sauer, "Critical review of the methods for monitoring of lithium-ion batteries in electric and hybrid vehicles," *Journal of Power Sources*, vol. 258, pp. 321–339, Jul. 2014.

[8] Y. Gao, X. Zhang, Q. Cheng, B. Guo, and J. Yang, "Classification and Review of the Charging Strategies for Commercial Lithium-Ion Batteries," *IEEE Access*, vol. 7, pp. 43 511–43 524, 2019.

[9] H. Beiranvand, N. Blasuttigh, T. Pereira, S. Hansen, H. Krueger, M. Liserre, and A. M. Pavan, "η_{max}-Charging Strategy for Lithium-Ion Batteries in V2G Applications," in *2022 IEEE Energy Conversion Congress and Exposition (ECCE)*. Detroit, MI, USA: IEEE, Oct. 2022, pp. 1–8.

[10] N. Blasuttigh, H. Beiranvand, T. Pereira, S. Castellan, A. Massi Pavan, and M. Liserre, "η_{max}-Charging Strategy for Lithium-Ion Batteries: Theory, Design, and Validation," preprint, Jul. 2023.

[11] Y. Wang, J. Tian, Z. Sun, L. Wang, R. Xu, M. Li, and Z. Chen, "A comprehensive review of battery modeling and state estimation approaches for advanced battery management systems," *Renewable and Sustainable Energy Reviews*, vol. 131, p. 110015, Oct. 2020.

[12] Q. Ouyang, J. Chen, J. Zheng, and H. Fang, "Optimal Multiobjective Charging for Lithium-Ion Battery Packs: A Hierarchical Control Approach," *IEEE Transactions on Industrial Informatics*, vol. 14, no. 9, pp. 4243–4253, Sep. 2018.

[13] Q. Ouyang, Z. Wang, K. Liu, G. Xu, and Y. Li, "Optimal Charging Control for Lithium-Ion Battery Packs: A Distributed Average Tracking Approach," *IEEE Transactions on Industrial Informatics*, vol. 16, no. 5, pp. 3430–3438, May 2020.

[14] A. Pozzi, M. Zambelli, A. Ferrara, and D. M. Raimondo, "Balancing-Aware Charging Strategy for Series-Connected Lithium-Ion Cells: A Nonlinear Model Predictive Control Approach," *IEEE Transactions on Control Systems Technology*, vol. 28, no. 5, pp. 1862–1877, Sep. 2020.

[15] Q. Ouyang, Y. Zhang, N. Ghaeminezhad, J. Chen, Z. Wang, X. Hu, and J. Li, "Module-Based Active Equalization for Battery Packs: A Two-Layer Model Predictive Control Strategy," *IEEE Transactions on Transportation Electrification*, vol. 8, no. 1, pp. 149–159, Mar. 2022.

[16] J. Chen, H. Chen, M. Zhou, L. Kumar, and J. Zheng, "Quadratic Programming-Based Simultaneous Charging Strategy for Battery Packs of Electric Vehicles," *IEEE/ASME Transactions on Mechatronics*, vol. 27, no. 6, pp. 5869–5878, Dec. 2022.

[17] Y. Yang, J. He, C. Chen, and J. Wei, "Balancing Awareness Fast Charging Control for Lithium-Ion Battery Pack Using Deep Reinforcement Learning," *IEEE Transactions on Industrial Electronics*, vol. 71, no. 4, pp. 3718–3727, Apr. 2024.

[18] A. Pozzi, M. Torchio, R. D. Braatz, and D. M. Raimondo, "Optimal charging of an electric vehicle battery pack: A real-time sensitivity-based model predictive control approach," *Journal of Power Sources*, vol. 461, p. 228133, Jun. 2020.

[19] X. Lin, H. E. Perez, J. B. Siegel, and A. G. Stefanopoulou, "Robust Estimation of Battery System Temperature Distribution Under Sparse Sensing and Uncertainty," *IEEE Transactions on Control Systems Technology*, vol. 28, no. 3, pp. 753–765, May 2020.

[20] Z. B. Omariba, L. Zhang, and D. Sun, "Review of Battery Cell Balancing Methodologies for Optimizing Battery Pack Performance in Electric Vehicles," *IEEE Access*, vol. 7, pp. 129 335–129 352, 2019.

[21] Z. Zhao, H. Hu, Z. He, H. H.-C. Iu, P. Davari, and F. Blaabjerg, "Power Electronics-Based Safety Enhancement Technologies for Lithium-Ion Batteries: An Overview From Battery Management Perspective," *IEEE Transactions on Power Electronics*, vol. 38, no. 7, pp. 8922–8955, Jul. 2023.

[22] M. Caspar, T. Eiler, and S. Hohmann, "Systematic Comparison of Active Balancing: A Model-Based Quantitative Analysis," *IEEE Transactions on Vehicular Technology*, vol. 67, no. 2, pp. 920–934, Feb. 2018.

[23] S. Barcellona and L. Piegari, "Effect of current on cycle aging of lithium ion batteries," *Journal of Energy Storage*, vol. 29, p. 101310, Jun. 2020.

[24] X. Lin, H. Fu, H. E. Perez, J. B. Siege, A. G. Stefanopoulou, Y. Ding, and M. P. Castanier, "Parameterization and Observability Analysis of Scalable Battery Clusters for Onboard Thermal Management," *Oil & Gas Science and Technology – Revue d'IFP Energies nouvelles*, vol. 68, no. 1, pp. 165–178, Jan. 2013.

[25] X. Hu, S. Li, and H. Peng, "A comparative study of equivalent circuit models for Li-ion batteries," *Journal of Power Sources*, vol. 198, pp. 359–367, Jan. 2012.

[26] M. Chen and G. Rincon-Mora, "Accurate electrical battery model capable of predicting runtime and I-V performance," *IEEE Transactions on Energy Conversion*, vol. 21, no. 2, pp. 504–511, Jun. 2006.

[27] Long Lam, P. Bauer, and E. Kelder, "A practical circuit-based model for Li-ion battery cells in electric vehicle applications," in *2011 IEEE 33rd International Telecommunications Energy Conference (INTELEC)*. Amsterdam, Netherlands: IEEE, Oct. 2011, pp. 1–9.

[28] S. Lucia, A. Tătulea-Codrean, C. Schoppmeyer, and S. Engell, "Rapid development of modular and sustainable nonlinear model predictive control solutions," *Control Engineering Practice*, vol. 60, pp. 51–62, Mar. 2017.

[29] J. A. E. Andersson, J. Gillis, G. Horn, J. B. Rawlings, and M. Diehl, "CasADi – A software framework for nonlinear optimization and optimal control," *Mathematical Programming Computation*, vol. 11, no. 1, pp. 1–36, 2019.

[30] A. Wächter and L. T. Biegler, "On the implementation of an interior-point filter line-search algorithm for large-scale nonlinear programming," *Mathematical Programming*, vol. 106, no. 1, pp. 25–57, Mar. 2006.